THE ASTROPHYSICAL JOURNAL, 198:493–505, 1975 June 1

A MEASUREMENT OF COSMIC-RAY POSITRON AND NEGATRON SPECTRA BETWEEN 50 AND 800 MV

J. K. DAUGHERTY,* R. C. HARTMAN, AND P. J. SCHMIDT†
Goddard Space Flight Center, Greenbelt, Maryland
Received 1974 May 31; revised 1974 September 30

ABSTRACT

A balloon-borne spark chamber magnetic spectrometer has been used to measure the spectra of cosmic-ray positrons and negatrons at energies between 50 and 800 MV. The data reported here were obtained during two flights from Fort Churchill, Manitoba, in 1972 July. The present results indicate that the dominance of negatrons from primary sources, found in earlier experiments above 200 MV, extends down to at least 50 MV. Solar modulation of the positron component is found to be consistent with that of the total electron spectrum, assuming that the positron component is entirely attributable to collisions between cosmic-ray nuclei and the interstellar gas.

Subject headings: abundances, cosmic ray — cosmic rays — interplanetary medium

I. INTRODUCTION

Knowledge of the spectra of cosmic-ray positrons and negatrons between 20 MV and 500 MV should provide valuable insight into the solar modulation of cosmic-ray electrons. Since it is possible to calculate with reasonable accuracy the interstellar spectrum of cosmic-ray positrons presumed to arise in collisions of cosmic-ray nuclei with the interstellar gas, a measurement of the cosmic-ray positron spectrum near the Earth provides a good estimate of the absolute solar modulation of the cosmic-ray electron component.

Several authors (Goldstein, Ramaty, and Fisk 1970; Cummings, Stone, and Vogt 1973*b*) have previously estimated the absolute solar modulation of cosmic-ray electrons by comparing measured total electron spectra with interstellar spectra derived from the measured nonthermal radio noise. This calculation is subject to substantial uncertainties, possibly as much as a factor of 4. In addition, the available radio measurements do not provide information on the electron spectrum below about 200 MV. Observation of the local interplanetary positron spectrum should provide a substantially more accurate estimate of the solar modulation while allowing the comparison to be carried to lower energies.

We report here the results of a balloon experiment designed to measure the separate spectra of cosmic-ray positrons and negatrons in the energy range between 20 and 500 MV. Several previous attempts have been made to carry out such investigations with balloon-borne experiments (Fichtel, Cline, and Kniffen 1968; Kniffen, Cline, and Fichtel 1970; Beuermann *et al.* 1969, 1970; Cummings *et al.* 1973*b*). However, several factors have combined to cause large uncertainties in those results. The primary difficulty is the separation of the primary positrons and negatrons from the large background of atmospheric secondary electrons. For this purpose, it is not only necessary to reach extremely high balloon altitudes; in addition, positron and negatron fluxes must be accurately measured over a wide range of atmospheric depths.

Because of the relatively low electron energies, the experiment must be performed at a high geomagnetic latitude. In fact, the geomagnetically northernmost location from which large balloons can be conveniently launched, Fort Churchill, Manitoba, is actually only marginally acceptable for the experiment. During the daytime, the geomagnetic cutoff at Fort Churchill is in the range of several hundred MV, limiting the useful portion of a balloon flight to the night hours, when the cutoff is below 20 MV (Hovestadt and Meyer 1970; Israel and Vogt 1969).

II. INSTRUMENT AND BALLOON FLIGHTS

Figure 1 is a schematic cross section of the spark chamber magnetic spectrometer used for this investigation. Sixteen spark chamber gaps define the trajectory of a charged particle before and after its passage through the gap of a permanent magnet. The direction and magnitude of the magnetic deflection determine the charge sign and rigidity of the particle.

Each of the 16 spark chamber modules (later referred to as decks) consists of two parallel 25 × 25 cm^2 grids of 0.01 cm beryllium-copper wires with a horizontal spacing of 0.127 cm. The wires of one grid are orthogonal to those of the other grid on the same module, so that both coordinates may be read out. Each wire threads a ferrite memory core whose state is changed whenever spark current flows in the wire, storing the information for later interrogation. The spark modules are separated into two "chambers" of eight decks each, one above and one below the magnet. Each chamber is divided into two tiers of four decks each, as indicated in Figure 1. The spark chamber gas used for these flights was a 90 percent neon–10 percent helium mixture, with 0.5 percent ethanol and 1 percent argon added, at a total operating pressure of 1 atm.

The master coincidence signal $C \cdot S_1 \cdot S_2 \cdot \langle A1 \rangle \cdot \langle A2 \rangle$,

* University of Maryland.
† NAS–NRC Postdoctoral Research Associate.

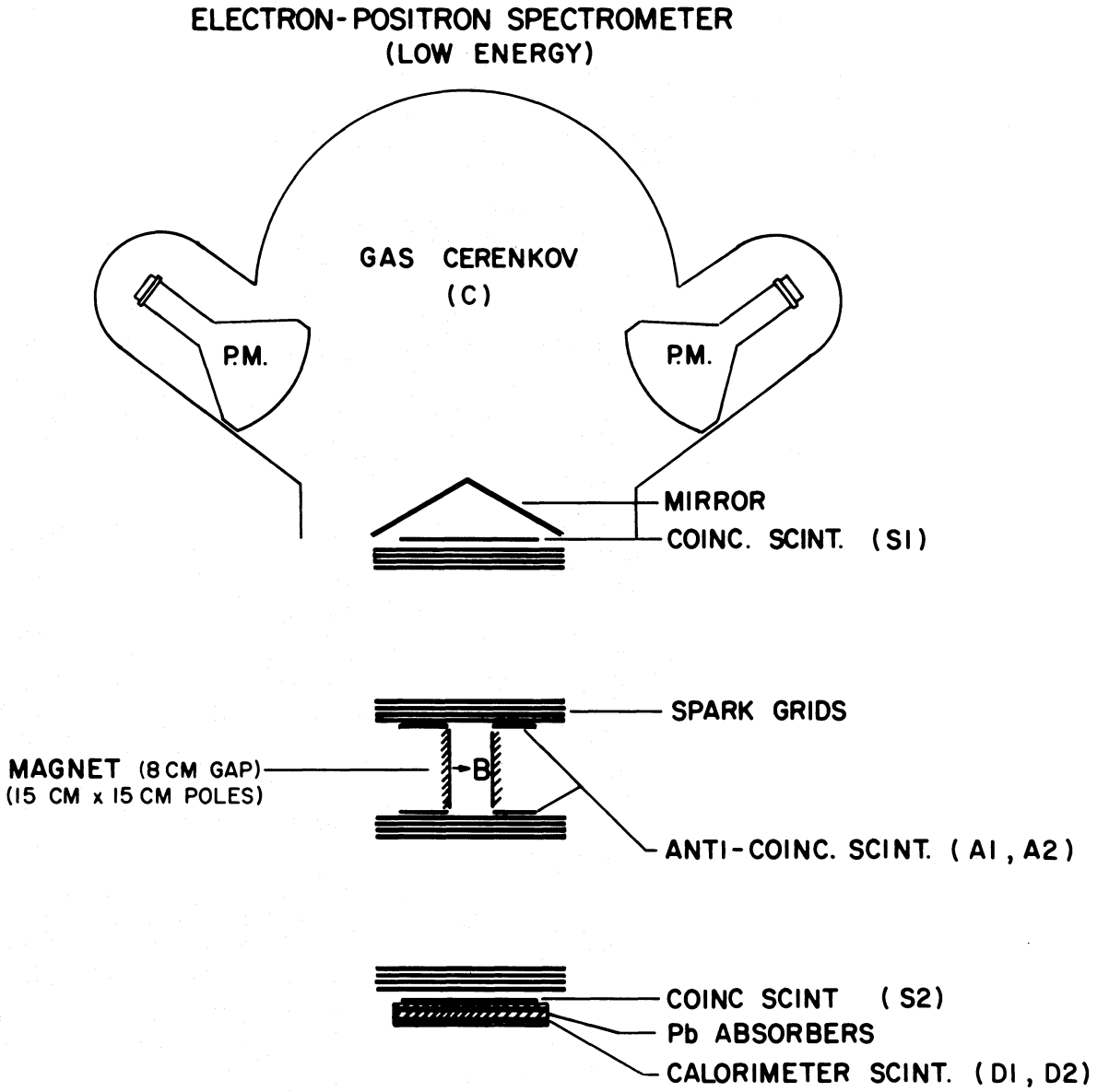

FIG. 1.—Schematic diagram of the detector

where $\langle\ \rangle$ means "not," is generated by a five-element particle telescope consisting of a gas Cerenkov counter C; two plastic scintillator counters S1 and S2, set to trigger on signals above about half that from a singly charged minimum ionizing particle; and two anticoincidence counters A1 and A2. This master coincidence causes the spark chamber to be triggered and read out (and gates the pulse-height analyzers for the shower counters described below).

The Cerenkov counter was filled with 1 atm of CO_2, providing a velocity threshold corresponding to $\gamma \approx E/mc^2 = 33$. The Cerenkov light is emitted at an angle no greater than 1°.7 from the particle path. For a downward-moving particle, the light is reflected by plane mirrors into two 22 cm photomultipliers outside the telescope field of view. The inside of the dome is painted black to absorb light produced by upward-moving particles.

The counters S1 and S2 are 25 × 25 cm² sheets of 0.475 cm plastic scintillator, each viewed by a single 5 cm photomultiplier tube. The anticoincidence counters, above and below the magnet, are plastic scintillators with 15 cm × 8 cm holes (the same dimensions as the magnet gap), each coupled by two adiabatic light pipes to two photomultiplier tubes located outside the spark gas enclosure.

The geometry of the telescope is determined by $S1 \cdot S2 \cdot \langle A1 \rangle \cdot \langle A2 \rangle$, with the Cerenkov counter providing only a velocity threshold and rejection of upward-moving particles. A geometrical factor of

19 cm^2 sr is obtained from a Monte Carlo calculation for rigidities above 50 MV. For lower rigidities the geometry factor is limited by deflection in the magnet; it becomes zero at about 15 MV. The permanent magnet has pole faces 15 × 15 cm^2 and a gap of 8 cm. Its central field is about 1 kilogauss, and it has a vertical line integral of about 25 kilogauss-cm.

In principle, the Cerenkov counter should not trigger on particles with $\gamma < 33$, and thus should reject all nucleonic cosmic rays in the rigidity range of interest here. However, the low light intensity produced by electrons traversing the Cerenkov gas requires that its discriminator have a very low threshold. This in turn produces a rather high (~ 5000 s^{-1}) counting rate due to dark noise in the two large photomultipliers. It is possible for a noise pulse from the Cerenkov counter to coincide (within the resolving time of 50 ns) with the passage of a low-energy proton (or other nuclear cosmic ray) through the telescope, generating a master coincidence signal. In order to separate these events from the positrons of interest, a shallow calorimeter is placed below the S2 counter. This subsystem contains two plastic scintillators (D1 and D2) at depths of 1 and 3 radiation lengths (rl) in a 4 rl stack of lead plates. Each of these scintillators is viewed, via an adiabatic light pipe, by a 7.5 cm photomultiplier whose output is digitized by a pulse-height analyzer when a master coincidence ($C \cdot S1 \cdot S2 \cdot \langle A1 \rangle \cdot \langle A2 \rangle$) occurs. A proton with rigidity below about 350 MV cannot penetrate even to D1, so requiring nonzero pulse height in either D1 or D2 effectively eliminates low-rigidity nucleons from consideration. The corresponding electron inefficiency, as well as the more complex criteria necessary for the 400–800 MV interval, are discussed later.

Data generated by the experiment were encoded and telemetered to the ground in a PCM (pulse code modulation) format at 12 kilobits s^{-1}. Three-quarters of the bit rate is available for spark chamber data, the rest being devoted to housekeeping data and telemetry synchronization. The housekeeping data contain single counting rates for the five telescope counters; the coincidence rates $C \cdot S1 \cdot S2 \cdot \langle A1 \rangle \cdot \langle A2 \rangle$, $S1 \cdot S2 \cdot \langle A1 \rangle \cdot \langle A2 \rangle$, and $C \cdot S1$; dead time; internal and external temperatures and pressures; and voltages and currents. A typical event contains about 700 bits of spark chamber data but requires a dead time of about 0.2 s because of the time required to scan the spark chamber core memory.

The first two flights of the instrument were launched during 1972 July from Fort Churchill, Manitoba. The launches were scheduled after 17:00 CST in order to avoid exposing the instrument during its ascent to the flux of reentrant albedo electrons, which is typically present between 06:00 and 18:00 (Jokipii, L'Heureux, and Meyer 1967; Israel and Vogt 1969; Hovestadt and Meyer 1970).

The first flight reached a float depth of 2.0 g cm^{-2}, remaining at nearly constant altitude for about 11 hours. The instrument performed well throughout this flight, although a leak in the gas Cerenkov counter pressure vessel (which appeared shortly after launch and persisted through most of the ascent before sealing itself off) reduced the CO_2 pressure to about 0.5 atm for the duration of the float period.

The experiment was later calibrated in an electron beam at the National Bureau of Standards electron synchrotron. This calibration allowed verification of the energy determination and measurement of the energy resolution and the detector efficiency as a function of Cerenkov gas pressure. In addition, it provided response distributions for the two shower counters.

During the second flight the instrument achieved a float depth of 2.5 g cm^{-2}. However, abnormally low temperatures in the detector electronics caused the master coincidence circuit to malfunction for a period during the latter part of the ascent data and the nighttime float. Although a temperature increase brought the coincidence circuit back to normal operation by 09:00 CST, the 3.5 hours of daytime float data gathered after that time were not used in the analysis.

The first flight has provided 9 hours of nighttime float data; useful atmospheric ascent data were obtained from both flights.

III. DATA ANALYSIS

An automatic track-identification technique was employed in the initial processing of the raw spark chamber event records. For each event, this program searches the list of set core addresses for straight track segments, and then classifies the event as accepted (in which case those core locations associated with the identified track are tagged), deleted, or questionable (requiring a display of the spark chamber data for visual inspection).

The automatically accepted events were required to show clean single tracks traversing all four spark chamber tiers. The Appendix describes in detail the criteria used in this selection. The automatically deleted events were those which showed, for instance, no set cores in a tier, no track through the two tiers in a chamber, etc.

Those events which could be neither accepted nor deleted by the automatic track-identification technique have been visually inspected and edited or deleted with the use of an IBM 1130/2250 computer graphics display. The procedure for the editing of an event allows the removal of core tags generated by the track-identification program, as well as the tagging of additional cores. The criteria used in this selection were relaxed somewhat to allow for δ-rays, spark chamber inefficiencies, etc. A more detailed description of the editing is given in the Appendix.

With the set of acceptance and rejection criteria described in the Appendix, the overall efficiency for the acceptance of spark events triggered by single electrons exceeds 90 percent, and is probably as high as 95 percent. Hence in the present analysis, the scanning acceptance efficiency has been assumed to be 95 ± 5 percent of all energies.

An exact expression for the rigidity ρ of a charged

particle traversing a static magnetic field may be written in the form

$$\rho = \frac{\int_i^f ds d\mathbf{r}/ds \times \mathbf{B}}{2 \sin \frac{1}{2}\theta}, \quad (1)$$

where θ is the angle between the tangential directions (in three-dimensional space) to the particle trajectory at two conveniently chosen points labeled i and f. The field path length integral is evaluated between these same points along the deflected trajectory.

In general, the evaluation of this expression requires a knowledge of the magnetic field vector at all points along a specified trajectory between i and f. As will be shown below, the fringe fields of the magnet in the present detector cannot be neglected in accurate rigidity estimates. Hence a detailed field map has been used in numerical determination of the field path length integral for each particle trajectory.

The deflection angle θ is determined from the slopes of the four straight line segments, obtained by least-squares fits to the tagged core locations. Two or more adjacent cores in a single deck are averaged to give a single point to be used in the fitting procedure. An iterative procedure is then used to remove points which have anomalously large deviations from the fit line, and a final check is made to ensure that enough points remain in each view to process the event.

Since the central field lies along the positive X-axis (with the Z-axis vertical), the relatively small deflection between X–Z views may here be neglected and θ may then be expressed simply as

$$\theta = \tan^{-1} \frac{|(dy/dz)_f - (dy/dz)_i|}{[1 + (dy/dz)_i(dy/dz)_f]^{1/2}}. \quad (2)$$

However, the presence of significant fringe fields within the spark chamber volume has required that the end-points i and f be chosen with caution. In particular, the slope of the straight line through each pair of tiers should be associated with the tangent to the true particle trajectory at some intermediate point between the two tiers. The location of this intermediate point depends on the relative strength and extent of the fringe fields, but is nearly independent of particle rigidity. Numerical integrations of particle equations of motion through the field of the detector have shown that the intermediate points lie near the plane $z = \pm 20$ cm. Hence these planes have been used as the limits of the field integration.

Since the rigidities of the particles in the spark event records are unknown beforehand, the exact trajectories through the magnetic field cannot be reconstructed by integrating the equations of motion. Hence an approximate trajectory must be assumed in the evaluation of the field integral. We have used as an approximate projected trajectory a segment of a circle which is tangent to both of the fit lines at the points i and f, respectively, and coincident with the upper projected segment at point i. Analysis of electrons of known energy from calibration of the instrument has indicated that this approximation technique introduces negligible errors for electron energies down to 50 MV.

The accuracy of rigidity measurements in the detector is limited both by the spark chamber spatial resolution and the random scattering of particles near the magnet gap region. Above several hundred MV the rigidity resolution is limited by the spark chamber spatial resolution ($\sim$0.05 cm), while at lower rigidities Coulomb scattering of particles near the magnet gap becomes the limiting factor. The rms (projected) scattering angle for a particle of rigidity ρ (measured in MV) which has traversed t radiation lengths of matter is given approximately by the expression (Moliere 1948)

$$\Delta\theta \approx \frac{15t^{1/2}}{\rho\beta}.$$

This equation has been used to estimate the scattering in the spark grid wires, the Mylar optical shielding planes, and the gas mixture throughout a central region encompassing both tiers nearest the magnet. For electrons the calculation has yielded the result

$$\Delta\theta \approx \frac{1.4}{\rho}.$$

Since the field integral is about 25 kilogauss-cm, the rigidity of a particle deflected by an angle θ is given approximately by

$$\rho \approx \frac{7.5}{\theta}.$$

The previous equations then imply that

$$\left|\frac{\Delta\theta}{\theta}\right| \approx \left|\frac{\Delta\rho}{\rho}\right| \approx 0.2.$$

Hence the relative uncertainty due to multiple Coulomb scattering should have a roughly constant value of about 20 percent.

The available calibration data for electrons between 50 and 140 MV indicate that the resolution is more nearly about 30 percent. This value may in fact be only an upper limit, since the energy dispersion of the beam may itself approach 30 percent. No more accurate determination of the beam energy dispersion is available to resolve this question.

The original line fits and rigidity estimates for the accepted events from each flight were used to correct for systematic errors in the relative alignment of the upper and lower spark chambers and in the horizontal positions of the individual grid modules. The fiducials used for this purpose were the trajectories of particles which produced minimum-ionizing pulse heights in both shower counters. These particles (which at float altitude are mainly protons above the gas Cerenkov counter threshold rigidity of 30 GV) should exhibit a well-defined peak at true angular deflections less than 1 milliradian. In the data from both flights, the observed peak in the y–z deflections has been found to be displaced by a few milliradians, indicating a slight misalignment of the spark chamber axes. As a

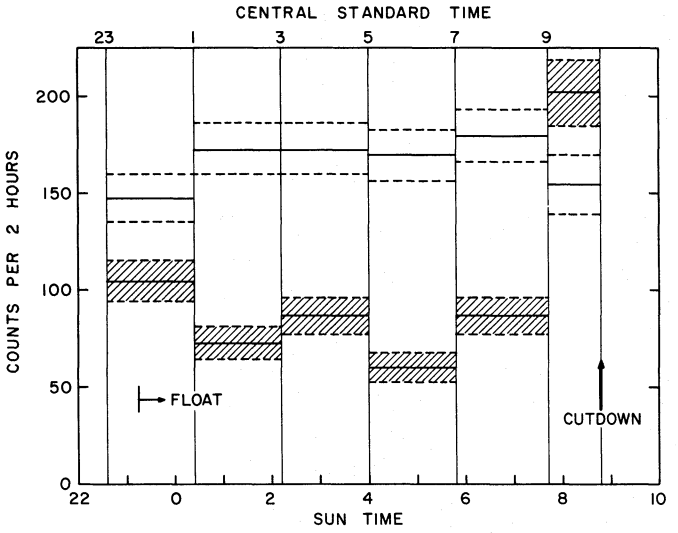

FIG. 2.—Raw counting rates for particles with rigidities below 100 MV (*shaded*) and 200–800 MV (*open*) during the float portion of the first flight.

first-order correction in iterated rigidity calculations, this observed displacement angle has been subtracted from the measured deflection angle for each event.

Net horizontal displacements in either the x or y directions for individual spark chamber modules have been found from histograms of the x- and y-coordinate deviations of each module from the fitted lines.

The measurable range of rigidities has been divided into the intervals 50–100, 100–200, 200–400, and 400–800 MV. The large intervals are used due to the limited numbers of particles counted during the time intervals of interest (typically 15 minutes during the ascent, since it is necessary to measure the positron and negatron intensities as functions of atmospheric depth).

The raw counting rates observed for particles in the rigidity intervals <100 and 100–200 MV during the first flight were examined in a search for the diurnal variation of the electron intensities. In the <100 MV interval, an abrupt rise by more than a factor of 2 was observed in the counting period which started at 09:00 CST, as shown in Figure 2. A less significant rise appeared in the 100–200 MV interval during the same period. Hence, for that flight, the onset of the daytime intensity increase has been assumed to occur about 09:00 CST.

Considerable care was used in determining positron and negatron fluxes as a function of altitude because of the instrument problems in both flights. Reduction of the Cerenkov pressure by about half during the first flight had the effect of reducing its detection efficiency, especially for electron energies below about 50 MV. One of the primary purposes of the instrument calibration was to measure the Cerenkov counter efficiency with gases of different indices of refraction. We have used air ($n = 1.00029$), CO_2 ($n = 1.00045$), and Freon 12 ($n = 1.00113$) in these measurements,

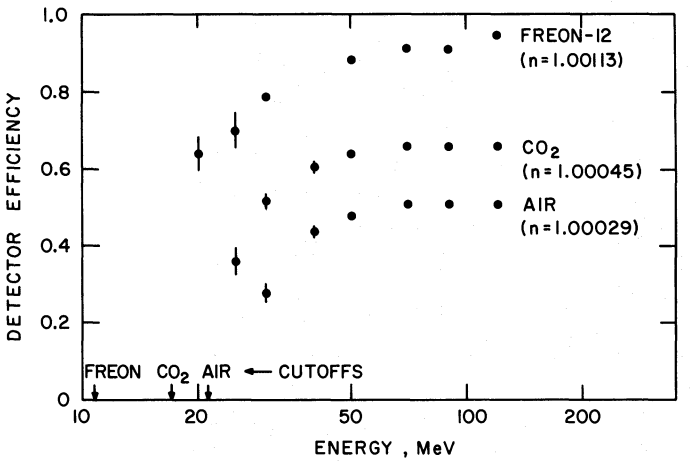

FIG. 3.—Measured detection efficiencies using various gases at a pressure of 1 atm

with the results shown in Figure 3. Since the index of refraction of CO_2 at the one-half atmosphere reached during the flight is slightly less than that of air, a short extrapolation was required to obtain the detector efficiency at that pressure. Since the Cerenkov pressure was changing during the ascent (fairly rapidly at first, then quite slowly for atmospheric depths less than 20 g cm^{-2}), a time-dependent efficiency was used in obtaining particle fluxes as a function of time (or atmospheric depth).

The coincidence circuit malfunction during the second flight was fairly sudden, and did not occur until the experiment had reached an atmospheric depth of about 10 g cm^{-2}. The particle fluxes as a function of depth obtained from the second flight have been used as a check on the time-dependent efficiency correction used for the first flight. The fluxes obtained for the two flights agree, within statistical limits, for all four energy intervals, and over the altitude range from 20 g cm^{-2} to 1000 g cm^{-2}.

The low Cerenkov counter detection efficiency for electrons below 50 MV during most of the first flight, as well as the lack of usable float data from the second, have prevented measurements of electron intensities below 50 MV. The upper limit is 800 MV, corresponding to a deflection of roughly 10 milliradians, since above this limit the uncertainty in the deflection angle measurement exceeds 30–40 percent.

The particle fluxes in each of the eight positive and negative rigidity intervals include a contribution from atmospheric secondary electrons, which is significant even at residual atmospheric depths as low as 2 g cm^{-2}. Several calculations of secondary electron intensities at various atmospheric depths and geomagnetic latitudes have been published (Perola and Scarsi 1966; Verma 1967; Beuermann 1971; Daniel and Stephens 1974), but the results depend on differing approximations and are not in complete agreement. Furthermore, the calculation of the absolute secondary electron intensities requires a knowledge of the time-dependent spectra of interplanetary protons and helium nuclei. The available calculations are in fact valid only for specified epochs in the solar cycle, and must be corrected for differences in the nucleonic cosmic-ray spectra at other epochs of interest.

As Beuermann (1971) has noted, however, two properties of the secondary electron intensities are not very sensitive to the temporal variations in the solar modulation of cosmic-ray nuclei. These parameters are the relative intensities of the positron and negatron components as functions of energy (the charge ratio), and the atmospheric depth dependence of these intensities within fixed energy intervals.

The depth dependence of the total (positive and negative) electron component has been measured in a number of previous balloon experiments (see, for example, L'Heureux 1967; Webber and Chotkowski 1967; L'Heureux and Meyer 1968; Simnet 1968; Bleeker *et al.* 1968). Most of these observations have been compared with assumed linear or near-linear growth curves for the secondary component as a means of estimating the primary intensity. Similarly, Beuermann *et al.* (1970) have compared the depth-dependence curves calculated by Beuermann (1971) for the separate positron and negatron intensities with magnetic spectrometer measurements between 12 and 220 MV. The search for significant departures from predicted secondary growth curves toward low atmospheric depths has, in fact, been generally considered the most reliable procedure for separating primary and secondary electron intensities in balloon measurements.

It must be noted, however, that recent calculations by Daniel and Stephens (1974) have resulted in secondary negatron growth curves which are not in agreement with the work of Beuermann (1971) at energies less than about 1 GV. The differences are most important at atmospheric depths less than 100 g cm^{-2}. Compared with the positron component, for which the two calculations give roughly similar results at all depths, the negatron intensities given by Daniel and Stephens (1974) decrease more rapidly with decreasing depth. Because of the theoretical uncertainties in the calculation by Daniel and Stephens (1974), which are in part due to inadequate accelerator data on $\pi^{\pm}$ energy distribution near the production thresholds, the results of Beuermann (1971) have been adopted in the present analysis. However, we have found that the primary negatron intensity above 200 MV is sufficiently high that the use of either set of growth curves leads to nearly identical results (within the statistical uncertainties). Between 50 and 200 MV, the larger secondary background implies that the primary negatron component obtained following Daniel and Stephens (1974) is roughly 1.4 times greater than that found using the results of Beuermann (1971), although this difference is still comparable to the statistical uncertainties in the present data at those energies.

The depth-dependence measurements of the positron intensities are complicated by a background of events due to low-rigidity nucleonic particles, mainly protons, which happen to be coincident with a noise pulse in the Cerenkov detector. These spurious events must be eliminated by using the pulse heights from the shower counters. The specific pulse-height restrictions imposed in the present analysis will be fully described below.

Estimates of the charge ratio require the use of identical pulse-height criteria in corresponding positive and negative rigidity intervals. Although the pulse-height restrictions introduce no systematic bias in the selection of positrons versus negatrons, a significant fraction of the electron events are rejected in all rigidity intervals. Within each interval the rejection is essentially independent of rigidity for the pulse-height criteria which have been imposed, but the statistical reliability of the depth-dependence measurements has been significantly degraded.

A finite measurement of the charge ratio has still proved feasible in the range below 400 MV. In the 400–800 MV range, however, the imposition of pulse-height criteria sufficient to eliminate all protons severely reduces the number of acceptable electron events, so only an upper limit can be obtained for the positive fraction. It has proven feasible to obtain the

negatron spectrum by relaxing the pulse-height criteria and confining attention to the intensities in the negative rigidity intervals. Using this negatron spectrum and the measured values of the positive fraction, it is possible to derive spectra for both the positrons and the total electron component. It has been possible to make comparatively reliable depth-dependence measurements of negatrons in each interval. These measurements will be discussed here to illustrate the depth-dependence analysis technique.

Figure 4 shows depth-dependence curves for several rigidity ranges. The error bars shown for each measurement include, in addition to the statistical errors, contributions from uncertainties in the Cerenkov counter efficiency and the scanning efficiency. The small uncertainties in the live time ($\lesssim 1\%$) and the geometric factor ($\pm 3\%$) have been neglected here.

The observed negatron intensity at any depth is the sum of primary and atmospheric secondary contributions. Hence the measured points in Figure 4 have been fitted to curves of the form

$$J(T, X) = a(T)p(T, X) + b(T)s(T, X) \qquad (3)$$

where $p(T, X)$ and $s(T, X)$ are specified functions which determine the depth dependence of the primary and secondary intensities, respectively. In the present analysis, the energy dependence of $p(T, X)$ and $s(T, X)$ has been averaged over each rigidity interval.

The depth dependence of secondary positrons and negatrons found by Beuermann (1971) may be approximated by two power-law curves, valid between 2–15 and 15–40 g cm^{-2}, respectively. The spectral indices in both depth intervals were calculated as functions of energy. Thus the shape of the secondary growth curves is fixed; b in equation (3) is the only free parameter in relating the secondary growth curves to given data points.

The depth dependence of the primary intensities must in principle reflect the distortion of the interplanetary electron spectrum by bremsstrahlung and collision losses in the residual atmosphere. Hence the shape of $p(T, X)$ depends on that of the interplanetary spectrum, which is unknown beforehand. As a first approximation, however, these losses may be ignored, and $p(T, X)$ may be given the highly convenient form $p(T, X) = 1$. The primary spectrum derived from equation (3) with this form for $p(T, X)$ may subsequently be traced through the residual atmosphere to obtain a better approximation for $p(T, X)$ (Beuermann 1971). The iterative procedure can be repeated until a self-consistent form for $p(T, X)$ is obtained. However, in the present analysis the first iteration has not significantly improved the fits to the available data.

In order to retain the maximum statistical reliability in the atmospheric depth-dependence measurements for each rigidity interval, it has been necessary to impose rigidity-dependent pulse height selection criteria. A numerical calculation has been used to estimate the relative energy losses and residual ranges of protons between 50 and 800 MV in the layers of the shower counter sandwich. The calculation provides estimates of the energy deposited in the two scintillators (labeled D1 and D2), as a function of proton (or heavier nucleus) rigidity. The results indicate that nucleonic particles below about 350 MV cannot penetrate the total amount of matter between the lower bulkhead and the first counter (D1). Hence in the rigidity intervals 50–100 and 100–200 MV, the nucleonic contamination may be removed by rejecting only those events which show no signal in both counters. This restriction eliminates 14 ± 4 percent of the negatrons in the 50–100 MV interval and 4 ± 4 percent in the 100–200 MV range. Since the threshold rigidity for penetration into D2 is about 440 MV, the contamination in the 200–400 MV interval may be eliminated by excluding events with no signal in the second counter. 14 ± 4 percent of the negatrons also fail this test. The possible residual contamination due to the finite rigidity resolution of the detector is negligible compared with the statistical uncertainties of the flight data.

The 400–800 MV interval is the only one requiring more stringent restrictions, since within this range protons may penetrate both scintillators and deposit energies equivalent to several minimum-ionizing particles in each counter. However, those protons which penetrate into D2 cannot produce more than about 6.0 times minimum-ionizing pulses in D1. Hence it is possible to remove the contamination between 400–800 MV by selecting only events with pulse heights above this value in D1 and some signal in D2. Only 30 ± 2 percent of the negatrons are retained after this restriction is imposed.

IV. RESULTS AND INTERPRETATIONS

The energy dependence of the positive fraction $N_+/(N_+ + N_-)$ in primary cosmic-ray electrons between 50 and 800 MV is shown in Figure 5. The earlier results obtained by Fanselow *et al.* (1969) over a slightly higher energy range have been included for comparison. The present measurements of the primary negatron intensities, derived from growth curves like those shown in Figure 4, have been combined with the corresponding values of the positive fraction to infer the primary positron intensities (shown in Fig. 6) as well as the total electron spectrum (Fig. 7).

As discussed above, the primary negatron and positron intensities found in this analysis have been derived using the growth curves for atmospheric secondary electrons given by Beuermann (1971). It has already been noted in the same discussion that at energies below about 200 MV, the use of recent atmospheric secondary calculations by Daniel and Stephens (1974) leads to primary negatron intensities which are about a factor of 1.4 higher than the results found in the present analysis. These differences are still comparable to the statistical uncertainties in the present data, but they may prove important in future measurements. However, above about 200 MV the differences in the theoretical growth curves become

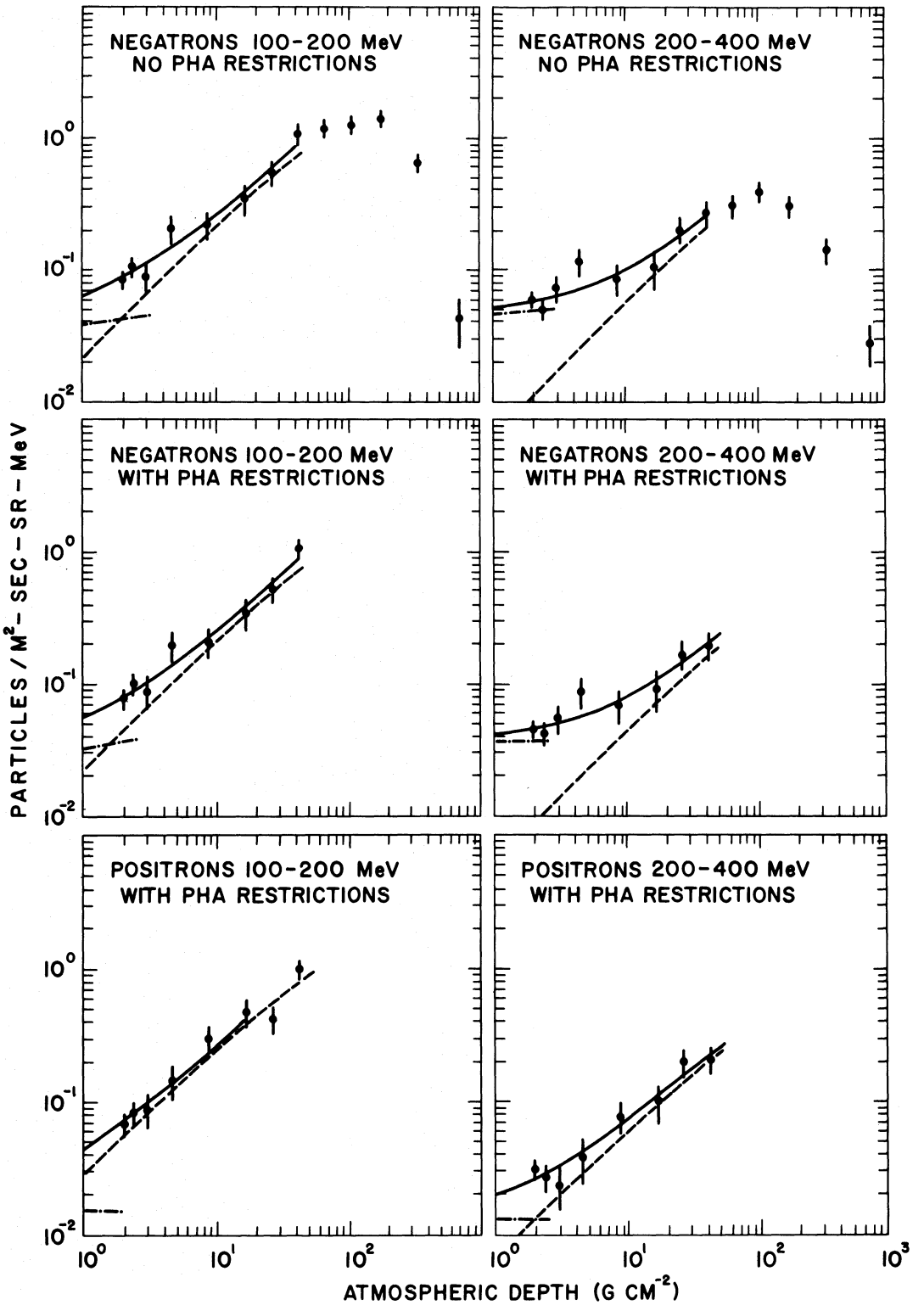

FIG. 4.—Representative atmospheric growth curves from the first flight. The restrictions referred to are described in the text.

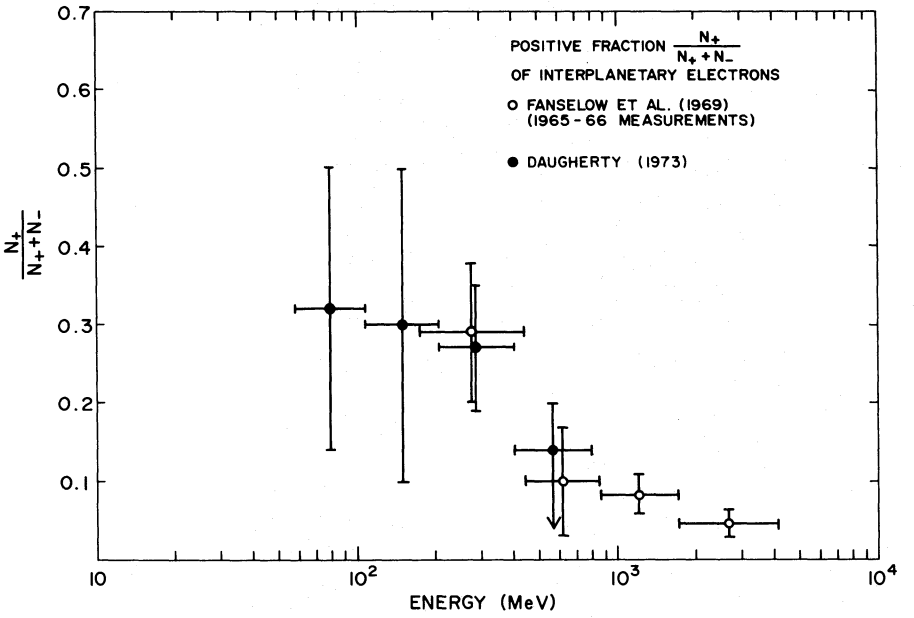

FIG. 5.—Positive fraction of interplanetary electrons, measured during the first flight

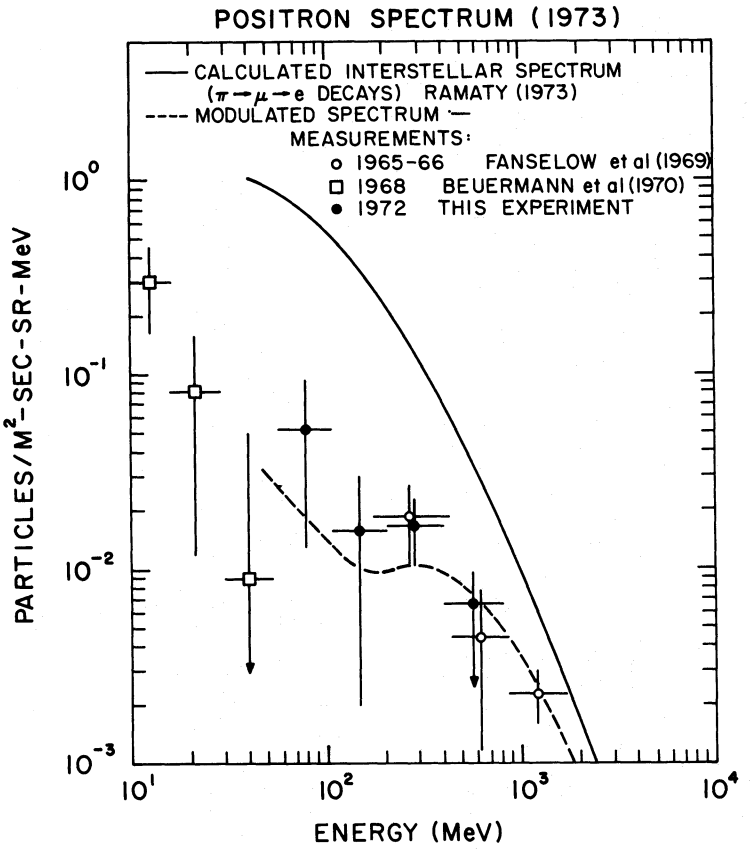

FIG. 6.—Positron spectrum

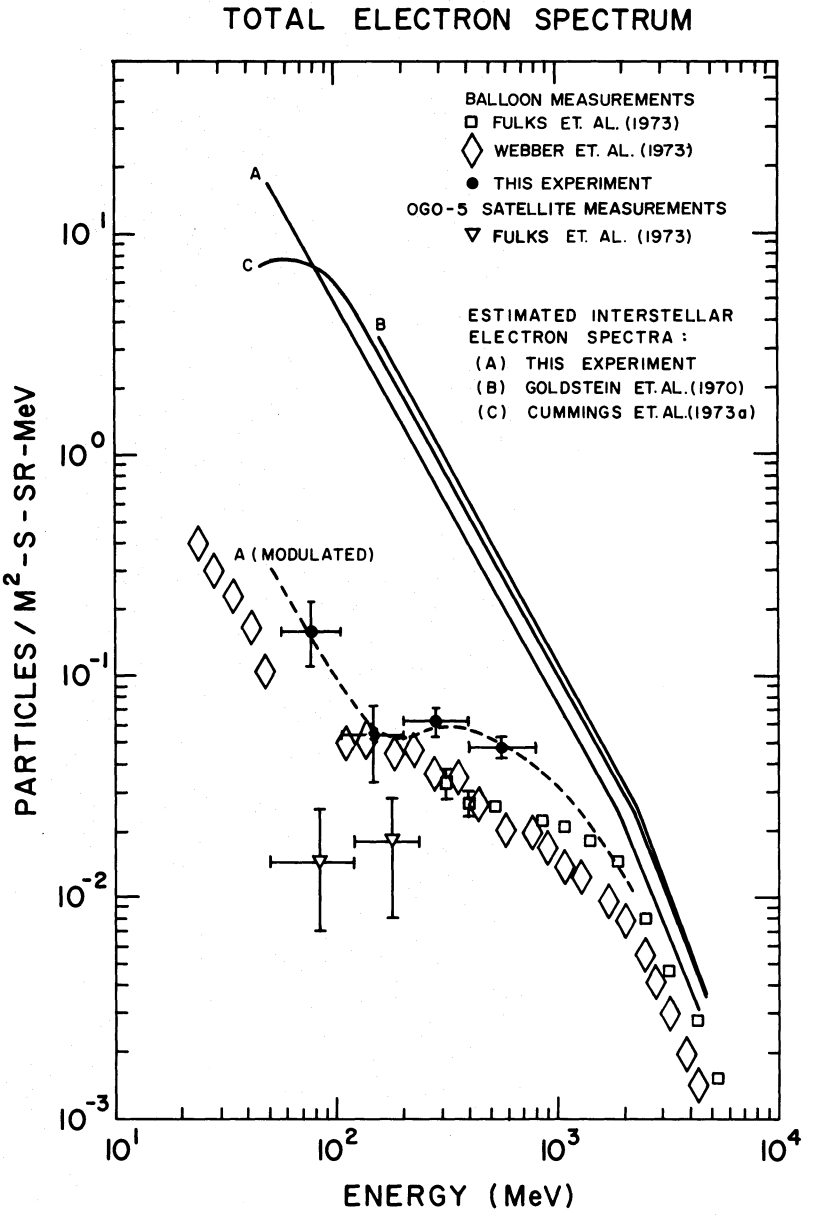

FIG. 7.—Total electron spectrum (1972 measurements)

less significant (since the contamination due to secondary electrons is considerably reduced); the two calculations lead to essentially similar results for the primary positron intensities.

Independent measurements reported by Webber *et al.* (1973) and by Fulks, Meyer, and L'Heureux (1973) for the total electron intensities in 1972 have also been included in Figure 7. Significant disagreements are apparent in these measurements. While the OGO 5 satellite results are lower than the other estimates below 200 MV, the intensities found in the present experiment are nearly a factor of 2 higher than the other balloon measurements above 200 MV (and apparently in the range 50–100 MV as well). The difference cannot result from dissimilar solar or geomagnetic conditions, since all three balloon experiments were flown from Fort Churchill during 1972 July. Neither brief solar disturbances nor significant variations in neutron monitor levels were recorded during any of these flights. The discrepancy is greater than could be accounted for by reasonable assumptions concerning uncertainties in the present experiment, in particular the time-dependent Cerenkov efficiency. It seems more likely that the disagreement

arises either from the significant differences in experimental technique, or procedures followed in the analysis of flight data.

The measurements of the separate cosmic-ray positron and negatron intensities have demonstrated that, at least between a few hundred MV and several GV, most of the electrons reaching the Earth from primary galactic sources are negatrons. Furthermore, at all energies above a few MeV, the modulated positron intensities observed near the Earth are consistently lower than the calculated interstellar spectra of galactic secondary electrons arising from $\pi \rightarrow \mu \rightarrow e$ decays (Ramaty 1973). While these facts do not by themselves exclude the possibility that positrons may be created and accelerated by some primary sources (for example, the model of pulsars suggested by Sturrock 1971), it is generally considered likely that the positron component above a few MV is entirely attributable to collisions of the cosmic-ray nucleonic component with interstellar gas.

If this assumption is valid, comparisons of measured positron intensities with the calculated galactic secondary positron spectrum may provide the most reliable measure of the absolute modulation of interstellar cosmic rays at a given epoch in the solar cycle. Although the positron measurements are, in general, more difficult than the observations of nucleonic cosmic rays, at present there is no reliable way to determine the interstellar spectra of nucleonic particles at the energies susceptible to significant modulation. To a lesser extent, the modulation of the total (positive and negative) electron component is also subject to considerable uncertainties, since the available estimates of the interstellar electron spectrum based on nonthermal radio observations (Goldstein *et al.* 1970; Cummings *et al.* 1973*b*) extend only from about 200 MV to several GV. Even in this range, the estimates are probably uncertain by at least a factor of 4 (Cummings *et al.* 1973*b*). However, from current knowledge of nuclear interactions and conditions in galactic space, the positron spectrum from interstellar $\pi \rightarrow \mu \rightarrow e$ decays is probably known to within a factor of 2 at all experimentally accessible energies above a few MV. Hence the absolute modulation of the positron spectrum over this entire range of energies may be estimated with comparative accuracy.

It is obvious that a quantitative test of the hypothesis that the positrons in this range are indeed predominantly of collisional origin would be of great significance. One method of testing this assumption is to compare the modulation of the positron component with that of the total electron component (Ramaty 1973; Cummings *et al.* 1973*a*). The present measurement of positrons and negatrons between 50 and 800 MV provides the basis for such a comparison, which has here been made in the context of the spherically symmetric model of the solar wind (Fisk 1971).

We have integrated numerically the complete interplanetary transport equation including the energy loss term, using the technique of Fisk (1971), with the aim of finding a single diffusion coefficient which can relate both the positron and total electron observations to assumed interstellar spectra of the forms given by Goldstein *et al.* (1970), and Ramaty (1973), respectively. It has been found that a diffusion coefficient of the form

$$K(r, \rho) = K_1(r)K_2(\rho)\,,$$

$$K_1(r) = \frac{1 + r}{1 + r^2}\,,$$

$$K_2(p) = 100Vr\rho\,, \qquad \rho > 0.25 \text{ GV}$$

$$= 25Vr\,, \qquad 0.05 \text{ GV} < \rho < 0.25 \text{ GV}$$

(where $V = 400$ km s^{-1} is the assumed solar-wind speed and r is measured in AU), and a boundary of 10 AU for the modulating region, give a consistent description of the modulation of both spectra down to 50 MV, as shown in Figures 5 and 6.

In order to match the available positron observations near 1 GV to the spectrum calculated by Ramaty (1973), the interstellar electron spectrum assumed here (curve A in Fig. 5) has been lowered slightly compared with the nominal values given by Goldstein *et al.* (1970) or Cummings *et al.* (1973*b*). However, this assumed spectrum is entirely consistent with the uncertainties estimated by these authors. In any case, a comparable, if somewhat smaller, uncertainty exists in the calculations of the positron spectrum (Ramaty 1973).

It should also be noted that the form of the electron spectrum adopted here obeys a simple power law with spectral index 1.8 at energies below 2 GV. No attempt has been made to incorporate a flattening of the spectrum below about 100 MV, as postulated by Cummings *et al.* (1973*a*) to account for the lower energy positron measurements of Beuermann *et al.* (1970). In the present analysis, the diffusion coefficient K has been chosen primarily to fit the shape of the modulated total electron spectrum, since the statistical uncertainties in the positron measurements are considerably greater. However, the resulting fit to the positron measurements in Figure 5 is obviously consistent with the assumption of a purely secondary origin for the positron component over this entire range of energies.

V. CONCLUSIONS

The present measurements of cosmic-ray positrons and negatrons have confirmed the results of previous experiments (Hartman, Meyer, and Hildebrand 1965; Hartman 1967; Fanselow *et al.* 1969), which demonstrated the existence of a dominant primary negatron component in the interstellar electron spectrum above a few hundred MV. In addition, finite estimates or upper limits have been established for the interplanetary positron and negatron spectra between 50 and 800 MV.

From a comparison of the measured intensities with independent estimates of the total interstellar electron spectrum (based on radio observations) and the interstellar positron spectrum resulting from $\pi \rightarrow \mu \rightarrow e$ decays in the Galaxy, consistent parameters have been

found to describe the solar modulation of both the positron and total electron intensities in 1972. Hence the positron measurements have been shown to be consistent with the hypothesis of a secondary origin for the positron component between 50 and 800 MV.

Further results of great value may be expected from future observations of cosmic-ray positrons and negatrons below 1 GV, as well as at higher energies. In addition to accumulating further significant information on the origins of galactic positrons and negatrons, such experiments can provide valuable constraints on the theory of solar modulation. Measurements of improved statistical accuracy might be used to monitor temporal variations in the positive fraction $N_+/(N_+ + N_-)$ as a function of energy. These observations may provide the most reliable verification of the adiabatic energy losses suffered by galactic cosmic rays penetrating the solar cavity. Finally, more precise estimates of the separate positron and negatron spectra may furnish new information on the interesting behavior of the interstellar electron spectra at energies below 100 MV.

In this context, it should be noted that the magnetic spectrometer which has obtained the measurements reported here may be expected to obtain results of considerably better statistical accuracy in forthcoming flights. It is hoped that significant improvements made in the detector system since the 1972 flights will ultimately permit accurate measurements of cosmic-ray positron and negatron spectra over the solar cycle.

We wish to thank A. Thompson, C. Ehrmann, and R. Smith for excellent design work; D. Andrews for technical assistance throughout the experiment preparation and balloon flights; and K. Harris and E. Greville for valuable contributions to the data processing and analysis effort. Discussions with Drs. L. Fisk, R. Ramaty, S. A. Stephens, and C. Fichtel have been extremely helpful. We are indebted to A. Filipovitch, W. Page, and Dr. S. Penner for their assistance with the instrument calibration at the National Bureau of Standards.

APPENDIX

EVENT ACCEPTANCE CRITERIA

Automatically accepted events must have exactly one track segment in each tier, and the slopes in each pair of tiers (above or below the magnet gap) must match within specified limits. A minimum of three set cores, in different decks, is required to identify a track segment in each tier, unless two cores in one tier are found close to the extrapolation of a segment from the other tier in the same chamber. In addition, there must be no anomalous deflection in the magnet gap region in the direction parallel to the magnetic field.

Events with more than one identifiable track segment in any tier, or too many set core locations not associated with any track, are tagged questionable, as are all events with significant deflections outside the magnet gap region. Only those events with no set cores in at least one tier, or too few points for satisfactory track identification in any tier, are automatically deleted.

The automatic track identification procedure was capable of accepting or deleting about 60 percent of the ascent data from each flight and a somewhat smaller portion of the float data. (It has recently been upgraded to about 95 percent efficiency.) An examination of a sample of 600 consecutive events from the ascent portion of Flight 72L2 revealed only three automatically accepted events which should have been edited to remove tagged cores (no more than one per event) which deviated by two to five core spacings from the apparent track segment. A similar inspection of the automatically deleted events (over 95% of which were rejected because at least one tier contained no track segment) showed no events which might have been acceptable after hand editing.

The acceptance criteria followed in hand editing the questionable events were straightforward, principally because the small amount of detector material above and within the spark chambers implies that electrons between 50 MV and 800 GV only infrequently exhibit large deflections or multiparticle tracks identifiable with knock-on or radiative collisions. Tracks whose rigidities could not be estimated because of obvious deflections (greater than about 5°) between a pair of tiers, or within a tier adjacent to the magnet gap, have necessarily been deleted. However, these lost events constituted less than 4 percent of the total number of questionable events. A somewhat larger percentage have been rejected because of anomalous deflections in the direction parallel to the magnetic field. In almost all of these cases the particles had apparently been scattered by a pole face of the magnet, and would not otherwise have satisfied the detector telescope requirements. Those events whose trajectories pass within 1 mm of the magnet pole faces are rejected later in the processing.

Small-angle scattering (especially less than three or four degrees) either within or between the tier projections is usually too difficult to observe on the display and must be estimated from the goodness-of-fit to the assumed straight trajectories calculated during the rigidity analysis.

Events with two or more apparent track segments in any tier of the spark chamber have in general been deleted, although two special classes of multiple-track events were edited and kept in the initial scanning sequence for each flight. The first class exhibited a principal track and one or more short accompanying tracks (not extending beyond the first tier) just below the Cerenkov counter bulkhead. Many of these tracks

could be attributed either to incipient electron showers or nucleonic cosmic-ray interactions above the upper spark chamber. These events were tentatively retained so that the shower counter pulse heights could be used to indicate those cases in which the single particle traversing both spark chambers could be identified as an electron. The second class of events displayed a principal track which appeared to produce a short range knock-on electron (δ-ray) in some tier without observable deflection. All events in these two classes which were eventually identified as electrons within the energy range 400–800 MV have been subjected to a second inspection. For this sample an error limit of 5 percent has been set on the percentage of erroneously accepted or hand-edited events.

Events in which multiple tracks appeared to emerge from the lower bulkhead have been rejected because of the likelihood that the tracks were due either to interacting cosmic-ray nuclei or to upward-moving particles. It should be noted that backward scattering may occasionally be observed in electron showers as well as nucleonic interactions. However, the event records from available electron calibration data suggest that this is a relatively infrequent occurrence, at least for energies up to 140 MV. In any case, the number of events rejected on this basis has not exceeded 3 percent of the inspected events.

Approximately 25 percent of the events which were included in the electron analysis had been inspected graphically. In the majority of these, the automatic event-recognition program was unable to complete analysis because of low spark chamber efficiency, or because of extraneous single sparks near the main track, probably caused by δ-rays. With the inclusion of these types, the events which are essentially "clean" constitute more than 90 percent of the total sample.

REFERENCES

Beuermann, K. P. 1971, *J. Geophys. Res.*, **76**, 4291.
Beuermann, K. P., Rice, C. J., Stone, E. C., and Vogt, R. E. 1969, *Phys. Rev. Letters*, **22**, 412.
———. 1970, *Acta Physica Academiae Scientiarum Hungaricae*, **29**, Suppl. 1, p. 173.
Bleeker, J. A. M., Burger, J. J., Deerenberg, A. J. M., Scheepmaker, A., Swanenburg, B. N., and Tanaka, Y. 1968, *Canadian J. Phys.*, **46**, S522.
Cummings, A. C., Stone, E. C., and Vogt, R. E. 1973*a*, *Proc. 13th International Conference on Cosmic Rays*, Denver, Colorado, **1**, 340.
———. 1973*b*, *ibid.*, p. 335.
Daniel, R. R., and Stephens, S. A. 1974, *Rev. Geophys. Space Phys.*, **12**, 233.
Fanselow, J. L., Hartman, R. C., Hildebrand, R. H., and Meyer, P. 1969, *Ap. J.*, **158**, 771.
Fichtel, C. E., Cline, T. L., and Kniffen, D. A. 1968, *Bull. Am. Phys. Soc.*, **13**, 1410.
Fisk, L. A. 1971, *J. Geophys. Res.*, **76**, 221.
Fulks, G., Meyer, P., and L'Heureux, J. 1973, *Proc. 13th International Conference on Cosmic Rays*, Denver, Colorado, **2**, 753.
Goldstein, M. L., Ramaty, R., and Fisk, L. A. 1970, *Phys. Rev. Letters*, **24**, 1193.
Hartman, R. C. 1967, *Ap. J.*, **150**, 371.
Hartman, R. C., Meyer, P., and Hildebrand, R. H. 1965, *J. Geophys. Res.*, **70**, 2713.
Hovestadt, D., and Meyer, P. 1970, *Acta Physica Academiae Scientiarum Hungaricae*, **29**, Suppl. 2, p. 525.
Israel, M. H., and Vogt, R. E. 1969, *J. Geophys. Res.*, **74**, 4714.
Jokipii, J. R., L'Heureux, J., and Meyer, P. 1967, *J. Geophys. Res.*, **72**, 4375.
Kniffen, D. A., Cline, T. L., and Fichtel, C. E. 1970, *Acta Physica Academiae Scientiarum Hungaricae*, **29**, Suppl. 1, p. 187.
L'Heureux, J. 1967, *Ap. J.*, **148**, 399.
L'Heureux, J., and Meyer, P. 1968, *Canadian J. Phys.*, **46**, 892.
Moliere, V. G. 1948, *Naturforschungen*, **3(a)**, 78.
Perola, G. C., and Scarsi, L. 1966, *Nuovo Cimento*, **46**, 718.
Ramaty, R. 1973, private communication.
Simnett, G. M. 1969, *Planet. Space Sci.*, **17**, 1781.
Sturrock, P. A. 1971, *Ap. J.*, **164**, 529.
Verma, S. D. 1967, *Proc. Indian Acad. Sci.*, **66A**, 125.
Webber, W. R., and Chotkowski, C. 1967, *J. Geophys. Res.*, **72**, 2783.
Webber, W. R., Kish, J., and Rockstroh, J. M. 1970, *Proc. 13th International Conference on Cosmic Rays*, Denver, Colorado, **2**, 760.

J. K. DAUGHERTY: 8 Munich 2, Bergmannstrasse 7, West Germany

R. C. HARTMAN: Code 662, NASA/Goddard Space Flight Center, Greenbelt, MD 20771

P. J. SCHMIDT: Winder Transportation Systems, Inc., Winder, GA 30680